# Pancreatic cancer organoids derived from EUS-guided fine needle aspiration specimens can be used to predict chemotherapy resistance.

**Soshi Oyama**
Department of Gastroenterology, Faculty of Medicine, Yamagata University
**Akiko Matsuda**
m.akiko@med.id.yamagata-u.ac.jp

Department of Gastroenterology, Faculty of Medicine, Yamagata University
**Yuko Murakami**
Division of multi-omics research, Yamagata University Well-being Institute
**Yasuharu Kakizaki**
Department of Gastroenterology, Faculty of Medicine, Yamagata University
**Tetsuya Ishizawa**
Department of Gastroenterology, Faculty of Medicine, Yamagata University
**Kazutoshi Kobayashi**
Department of Gastroenterology, Faculty of Medicine, Yamagata University
**Hitomi Nakamura**
Department of Gastroenterology, Faculty of Medicine, Yamagata University
**Yoshihito Nawa**
Department of Gastroenterology, Faculty of Medicine, Yamagata University
**Yu Otaki**
Department of Gastroenterology, Faculty of Medicine, Yamagata University
**Yamato Nagata**
Department of Gastroenterology, Faculty of Medicine, Yamagata University
**Soichiro Honma**
Department of Gastroenterology, Faculty of Medicine, Yamagata University
**Naohiko Makino**
Department of Gastroenterology, Faculty of Medicine, Yamagata University
**Hidenori Sato**
Division of multi-omics research, Yamagata University Well-being Institute
**Yoshiyuki Ueno**
Department of Gastroenterology, Faculty of Medicine, Yamagata University

**Article**

**Keywords:** pancreatic cancer, organoids, drug screening, biomarkers

**Posted Date:** July 18th, 2024

**DOI:** https://doi.org/10.21203/rs.3.rs-4600001/v1



**Additional Declarations:** No competing interests reported.

# Abstract

Pancreatic ductal adenocarcinoma (PDAC) has a poor prognosis. Although chemotherapy has become increasingly important in recent years, there are no practical markers to predict therapeutic efficacy. Here, we have aimed to identify novel markers that predict resistance to chemotherapy drugs using patient-derived organoids (PDOs) of PDAC. PDOs were established using endoscopic ultrasound - guided fine needle aspiration (EUS-FNA) specimens. Drug sensitivity tests were performed on 15 PDOs and the correlation between drug sensitivity and transcriptome analysis were evaluated. *BARD1* and *RAD50* have been identified as genes associated with gemcitabine resistance. Additionally, *SLC25A10* and *MAP3K9* were identified as genes associated with gemcitabine + paclitaxel resistance.PDOs derived from EUS-FNA specimens can be used to assess individual drug resistance and to identify predictive factors for chemotherapy resistance.


# Introduction

Pancreatic ductal adenocarcinoma (PDAC) has a poor prognosis and it is the third leading cause of cancer-related deaths with a five-year survival rate of only 12%[1]. Although it is difficult to improve outcomes with surgery alone, neoadjuvant chemotherapy (NAC) has been proposed as a new treatment method for PDAC and is now recognized as the preferred approach for borderline resectable (BR) PDAC according to the 2022 NCCN guidelines[2]. Recent cohort studies have indicated the effectiveness of NAC in both resectable and BR PDAC[3–5]. Thus, NAC is becoming increasingly important for improving the prognosis of PDAC; however, current treatment regimens are still insufficient, and there are no practical markers to predict the response to chemotherapy[6]. Therefore, there is a clear need to develop more effective pharmacological therapies and discover useful markers for predicting drug sensitivity.

"Organoids" are artificially created tissues that resemble organs[7]. Leading experts in the organoid research field define the term organoid as follows: an organoid is a three-dimensional structure derived from (pluripotent) stem cells, progenitors, and/or differentiated cells that self-organize through cell-cell and cell-matrix interactions to recapitulate aspects of the native tissue architecture and function *in vitro*[8]. In 2015, the feasibility of culturing tumorous lesions was demonstrated as human and mouse pancreatic cancer organoids. These maintained their histological properties and they have already been used in research[9].

Endoscopic ultrasound-guided fine needle aspiration (EUS-FNA) has used for the histological diagnosis of PDAC. Organoids derived from EUS-FNA specimens enable the genetic analysis of PDAC[10]. In recent years, it has been reported that drug sensitivity can be evaluated by administering chemotherapeutic drugs to PDAC organoids derived from EUS-FNA samples[11], and their application in personalized medicine is expected.

This study has aimed to evaluate the availability of patient-derived organoids (PDOs) in drug sensitivity tests and identify markers associated with drug resistance. We generated PDOs from EUS-FNA

specimens of patients with PDAC and performed drug sensitivity tests by administering chemotherapeutic drugs to these PDOs. Based on the drug sensitivity results, we performed transcriptomic analysis to evaluate the expression of genes associated with gemcitabine (GEM) or gemcitabine + paclitaxel (GEM + PTX) resistance and explored predictive markers for GEM or GEM + PTX resistance.

## Results

# Patient characteristics

We attempted to create PDAC organoids from the EUS-FNA specimens with a confirmed diagnosis of adenocarcinoma in 47 cases; their characteristics are shown in Table1. PDOs were successfully established in 32 cases and grown to confluence in 17 cases. These 17 cases were classified as the well growth group and 30 cases that failed to grow to confluence were classified as the poor growth group; the clinical characteristics between them were compared, but no clear significant difference was observed *(P value < 0.05*). The group with good growth was subjected to a drug sensitivity test; however, 2 cases were excluded from the study. One case had poor growth after thawing and the other had a bacterial infection. Drug sensitivity tests were performed in 15 cases, and their characteristics are shown in Table2.

Table 1

Background on all cases attempted establishment of organoids. Data were presented as number (percentage) of patients unless otherwise indicated. Abbreviations: EUS-FNA, Endoscopic ultrasonic fine needle aspiration. *BMI is the weight in kilograms divided by the square of the height in meters.

| **Variables** | **Overall(n = 47)** |
|---|---|
| **Age, yr** | 69 (49–79) |
| **Famale sex** | 20 (43) |
| **BMI*, kg/m$^2$** | 22 (16–30) |
| **TNM staging by UICC (8th)** | |
| I | 7 (15) |
| II | 8 (17) |
| III | 7 (15) |
| IV | 25 (53) |
| **Location** | |
| head | 14 (30) |
| body | 19 (40) |
| tail | 14 (30) |
| **Tumor size, mm** | 33 (12–80) |
| **EUS-FNA** | |
| punctures, count | 3.7 (3–5) |
| cytodiagnosis | |
| positive | 29 (62) |
| suspicious | 13 (28) |
| negative | 5 (11) |
| histological examination | |
| positive | 31 (66) |
| suspicious | 6 (13) |
| negative | 10 (21) |
| **Organoid culture** | |

| Variables | Overall(n = 47) |
|---|---|
| established | 32 (68) |
| confluent | 17 (36) |

Table 2
Background of 15 organoid cases with drug sensitivity testing

| Variables | Overall(n = 15) |
|---|---|
| Age, yr | 70 (50–79) |
| Famale sex | 8 (53) |
| BMI*, kg/$m^2$ | 21 (17–30) |
| TNM staging by UICC (8th) | |
| I | 2 (13) |
| II | 2 (13) |
| III | 3 (20) |
| IV | 8 (53) |
| Location | |
| head | 4 (27) |
| body | 7 (47) |
| tail | 4 (27) |
| Tumor size, mm | 33 (12–80) |
| EUS-FNA | |
| punctures, count | 3.7 (3–5) |
| cytodiagnosis | |
| positive | 10 (67) |
| suspicious | 3 (20) |
| negative | 2 (13) |
| histological examination | |
| positive | 10 (67) |
| suspicious | 3 (20) |
| negative | 2 (13) |

Data were presented as number (percentage) of patients unless otherwise indicated. Abbreviations: EUS-FNA, Endoscopic ultrasonic fine needle aspiration. * BMI is the weight in kilograms divided by the square of the height in meters.

# PDOs show pathological and genetic homology with donor tumor

Pathological evaluation of the PDOs (H8 and H9) was performed. HE staining of H8 and H9 cases revealed tumor cells with large nuclei and irregular ductal structures, which was consistent with the histology of the EUS-FNA specimen (Fig. 1A, B).

A comprehensive cancer panel (CCP) analysis showed that all of the 15 PDOs harbored *KRAS* mutations. Other mutations were observed in *TP53* (47%), *TNFRSF14* (20%), *RET* (13%), *TSC2* (13%), *SF3B1* (7%), and *SMAD4* (7%) (Fig. 1C). In pancreatic cancer, *KRAS* and *TP53* mutations are representative driver mutations[13–15], and it has been concluded that these PDOs show pathological and genetic homology with pancreatic cancer.

# Evaluation of drug sensitivity test for PDOs

Drug sensitivity tests were performed on 15 PDOs derived from EUS-FNA specimens to evaluate their response to three chemotherapeutic drugs: GEM, PTX, and GEM + PTX (Fig. 2A-C). Among the 15 PDOs, there were strains with various passage numbers, and the cryopreserved PDOs were stably recultured after thawing. The dose-response curve of the PDOs differed among the organoid strains, indicating individual differences in drug sensitivity. In drug sensitivity test for GEM and GEM + PTX, two PDO strains, H32 and H17, maintained approximately 50% cell viability even at drug administration with high dosage. This indicates that these two PDOs were resistant to GEM and GEM + PTX.

Normalized AUCs were generated from each dose-response curve, with high normalized AUC values indicating low drug sensitivity, and the low values indicating high sensitivity. The violin plot shows the normalized AUCs of PDOs treated with GEM, PTX, or GEM + PTX (Fig. 2D). Drug sensitivity tests were performed at similar drug concentration ranges in the GEM and GEM + PTX groups. The normalized AUC values were significantly lower in the GEM and GEM + PTX groups than in the PTX group (P value < 0.01). There was no statistically significant difference between the GEM and GEM + PTX groups; however, there was a trend toward lower normalized AUC values in the GEM + PTX group.

# Evaluation of the transcriptional changes associated with GEM or GEM + PTX resistance

We obtained the transcripts of 4,880 genes from 15 PDOs using transcriptome analysis. Using the obtained log10(TPM), Pearson correlation analysis was performed with the normalized AUC values of each drug sensitivity analysis result to identify the genes with a P value *< 0.001*. Among the genes correlated with the normalized AUC, 37 were identified in the GEM group, 6 in the PTX group, and 12 in the GEM + PTX group.

NMF analysis was performed on the identified genes in each group. In the GEM group, 37 genes were classified into two groups: basis1 and basis2. The basis1 gene group was associated with high normalized AUC values and low drug sensitivity, whereas the basis2 gene group had low normalized AUC values and high drug sensitivity (Fig. 3A). GO enrichment analysis and pathway enrichment analysis were performed on characteristic genes in the basis1 gene group (framed blue in Fig. 3A) associated with drug resistance (supplementary Table s1,s2). In the biological processes (BP) of the GO terms involved

in the regulation of cancer cell growth, such as DNA damage repair, cell cycle regulation, and replication fork processing, *BARD1* and *RAD50* were identified as significant factors (Fig. 3B, C). Regression analysis revealed a positive correlation, in which the normalized AUC value increased as the expression levels of *BARD1* and *RAD50* increased (Fig. 3D, E). For both *BARD1* and *RAD50*, normalized AUC values correlated with gene expression levels, indicating that high expression levels of these genes correlate with GEM resistance.

NMF analysis was performed on the 12 genes identified in the GEM + PTX group (Fig. 4A). GO enrichment analysis and Pathway enrichment analysis (supplementary Table s3, s4) were performed on the basis1 gene group (framed in blue in Fig. 4A). *SLC25A10* was identified in both GO enrichment analysis and pathway enrichment analysis. *MAP3K9*, a factor involved in the mitogen-activated protein kinase (MAPK) pathway, was also observed by GO enrichment analysis (Fig. 4B, C). Regression analysis revealed a positive correlation, in which the normalized AUC value increased as the expression levels of *SLC25A10* and *MAP3K9* increased (Fig. 4D, E). NMF and enrichment analyses were performed on the six genes identified in the PTX group; however, no genes associated with drug resistance were identified.

We also performed a multiple regression analysis in order to determine whether the combination of genes extracted in the NMF analysis was associated with stronger drug resistance. First, for the basis1 group in the GEM group, we focused on six genes that were significant in the GO enrichment analysis. It was confirmed that *PPP1R10* expression was added to the combination of *BARD1* and *RAD50* (*P value = 0.000049*, $R^2$ = 0.9095) or *SRSF6* (*P value = 0.000056*, $R^2$ = 0.9074) expression, which was associated with normalized AUC values, namely, GEM resistance. Also, on the basis1 gene group in the GEM + PTX group, we focused on the 5 genes that were found to be significant in the GO enrichment analysis. The combination of *SLC25A10* and *MAP3K9* expression (*P value = 0.000015*, $R^2$ = 0.8926) had a higher association with the normalized AUC value, namely, GEM + PTX resistance.

# Discussion

In the present study, we performed drug sensitivity tests and transcriptome analyses of PDOs obtained from EUS-FNA specimens to identify markers for evaluating drug resistance. We identified some markers associated with resistance to GEM and GEM + PTX; among them, *BARD1* and *RAD50* were considered potential predictors of GEM resistance in PDAC.

GEM, 2',2'-difluoro 2'-deoxycytidine (dFdC), is a deoxycytidine analog and utilized for treating several cancers. In PDAC, it are most classical chemotherapeutic agents[16]. GEM is metabolized within cells to form the nucleotides gemcitabine diphosphate (dFdCDP) and triphosphate (dFdCTP), which have been shown to exhibit cytotoxic effects by inhibiting DNA synthesis[17, 18]. In addition, dFdCTP competes with deoxycytidine triphosphate (dCTP) to induce apoptosis after incorporation into the DNA strand by DNA polymerase[19]. In other words, GEM inhibits DNA synthesis by incorporating into DNA strands and exhibits anticancer effects.

BARD1 forms a heterodimer with BRCA1 via its N-terminal RING domains[20]. It has been suggested that BRCA1 directly binds to DNA and promotes DNA repair[21]; however, BARD1 has also been found to bind to DNA and contribute to the DNA-binding ability of the BRCA1-BARD1 complex[22]. BARD1 and BRCA1 are highly expressed in tamoxifen-resistant breast cancer cells, suggesting that they resist DNA-damaging chemotherapy by enhancing DNA damage repair[23]. RAD50 forms the MRE11-RAD50-NBS1 (MRN) complex and plays an important role in DNA damage response. The MRN complex is the core conductor of early and sustained responses to DNA double-stranded breaks, replication fork stalling, telomere dysfunction, and viral DNA infection[24]. Additionally, the MRN complex may contain replication fork surveillance or DNA repair mechanisms that respond to chemotherapeutic drug-induced replication inhibition and may contribute to drug resistance[25]. Therefore, it is considered that the increased expression of *BARD1* and *RAD50* improves DNA repair ability and also suppresses the induction of cell death, possibly resulting in GEM resistance. *BARD1* and *RAD50* are potential predictive markers of GEM resistance.

Additionally, it was confirmed that the combination of *BARD1* and *RAD50* expression added to *PPP1R10* or *SRSF6* expression showed a higher association with normalized AUC values; PPP1R10 is a protein phosphatase 1 (PP1) nuclear-targeting subunit that responds to DNA damage involved in DNA repair[26, 27]. SRSF6 activates DNA damage response pathways such as DNA repair and double-strand break repair by regulating alternative splicing[28]. In addition to BARD1 and RAD50, multiple DNA repair-related genes may synergistically confer GEM resistance in PDAC.

We identified *SLC25A10* and *MAP3K9* as potential predictors of GEM + PTX resistance in PDAC. The SLC25 family of nuclear-encoded transporters located in the inner mitochondrial membrane is involved in many metabolic pathways and cellular functions[29]. SLC25A10 is also a dicarboxylate carrier that transports malate and succinate out of mitochondria in exchange for phosphate, sulfate, and thiosulfate[30, 31]. Overexpression of SLC25A10 has been associated with decreased overall survival in lung cancer and breast cancer patients[32]. It has also been suggested that SLC25A10 may confer cisplatin resistance by protecting tumor cells from oxidative stress[33].

MAP3K9 (mitogen-activated protein kinase kinase kinase 9), also known as mixed-lineage kinase 1 (MLK1), is an important upstream component in the MAPK pathway[34, 35]. It has been suggested that MAP3K9 enhances PDAC cell growth and partially inhibits cell apoptosis through activation of the MEK/ERK and NF-kB pathways[36]. MLK1 inhibitors have been shown to inhibit the growth of pancreatic cancer cell lines[37]. These results suggest that SLC25A10 is involved in tumor protection and MAP3K9 is involved in tumor growth, and the increased expression of *SLC25A10* and *MAP3K9* shown in this study may contribute to GEM + PTX resistance.

This study had three limitations. First, although 32 PDOs were established, a drug sensitivity test was performed on 15 PDOs with good growth; PDOs with insufficient growth were excluded. Second, the short observation period of patients for whom PDOs were established made it difficult to assess the

correlation between patient outcomes and the results of drug sensitivity tests. Third, the study had to be performed in the absence of cancer-related fibroblasts (CAFs), which is an important requirement for drug sensitivity assessment. In future, we plan to conduct drug sensitivity tests using more PDOs and evaluate their relationships with patient outcomes. In addition, to reproduce the tumor microenvironment, we are planning to use a co-culture model of PDOs and CAFs[38, 39] in order to regulate the expression of the identified genes and evaluate the changes in drug sensitivity.

In conclusion, we have performed drug sensitivity tests and transcriptome analysis of PDOs obtained from EUS-FNA specimens and identified *BARD1* and *RAD50* as predictive markers associated with GEM resistance and *SLC25A10* and *MAP3K9* as predictive markers associated with GEM + PTX resistance. PDOs have the potential to evaluate chemotherapeutic drug sensitivity and predict markers of drug resistance to chemotherapeutic drugs clinically.

## Methods

# Human pancreatic cancer samples

The participants were patients with pancreatic cancer who underwent EUS-FNA at Yamagata University Hospital between March 2020 and March 2023. This study was approved by the Ethics Committee of Yamagata University Hospital. All experiments were performed in accordance with the Declaration of Helsinki and the Commission guidelines and regulations. We obtained informed consent from all the participants in accordance with Ethical guidelines for life science and medical research involving human subjects. Also, the specimens and the data provided from the participants were stored, in accordance with the same ethical guidelines, immediately converted into a state that does not allow for the identification of individuals, and password-protected.

# EUS-FNA

This procedure was performed using a convex ultrasonic endoscope (GF-UCT260; Olympus, Japan) equipped with an ultrasound endoscopic puncture needle (AcquireTM 22G; Boston Scientific, USA). The puncture needle was moved back and forth 20 times per session, and 2–4 sessions were performed for each patient. After puncturing, the specimen was removed with a stylet, and tumor cells were confirmed by rapid on-site evaluation (ROSE). If tumor cells were detected by ROSE, the procedure was terminated, and PDOs were created from the surplus specimen.

# Organoid culture

PDOs were cultured with slight modifications to the method described by Seino et al.[12]. The FNA samples were incubated with Red Blood Cell Lysis Buffer (Roche) to remove the red blood cells. The resulting pancreatic cancer cells were embedded in Matrigel and cultured in Advanced DMEM/F12 supplemented with penicillin/streptomycin, 10 mM HEPES, 2 mM GlutaMAX, 1×B27 (Thermo Fisher Scientific), 10 nM gastrin I (Sigma-Aldrich), and 1mM N-acetylcysteine (Wako, Japan). The culture

medium was supplemented with the following niche factors: 100 ng/ml mouse recombinant noggin (Peprotech), 10% R-spondin-1 conditioned medium, 25% Afamin-Wnt-3A serum-free conditioned medium, 500 nM A83-01 (Tocris).

# Pathological analysis

The prepared PDOs were solidified into a jelly according to the protocol of iPGell (GenoStaff, Japan). They were then fixed in 10% neutral buffered formalin, and tissue blocks were created. Thin sections were prepared from tissue blocks, stained with hematoxylin and eosin (HE), and pathologically evaluated.

# Drug sensitivity test

PDOs were disassembled into single cells and seeded at 3000 cells per well in a 96-well plate. The chemotherapy drugs used were gemcitabine (GEM), paclitaxel (PTX), and gemcitabine + paclitaxel (GEM + PTX). GEM + PTX was mixed at a GEM: PTX ratio of 8:1. The concentration range of each is $1.0\times10^{-8}$ M to $2.0\times10^{-2}$ M for GEM, $1.0\times10^{-8}$ M to $2.6\times10^{-3}$ M for PTX, and $1.0\times10^{-8}$ M to $2.3\times10^{-2}$ M for GEM + PTX. Each drug was administered in duplicates. After incubating the plate treated with chemotherapy drugs at 37°C for 72 hours, 20 µl per well of CellTiter-Glo Cell Viability Assay (Promega) was added and incubated in the dark for 4 hours. The number of viable cells was assessed by measuring fluorescence using a Varioskan LUX multimode microplate reader (Thermo Fisher Scientific). Cell viability was calculated at each concentration using the minimum concentration as the reference value.

# Drug sensitivity analysis

A dose-response curve (top 1, bottom 0) was derived from cell viability, and the area under the curve (AUC) was calculated using GraphPad Prism 9 (GraphPad Software). The normalized AUC values were calculated by dividing the AUC by the AUC of the maximum concentration, and the normalized AUC values of each drug were divided into three groups and then compared.

# Extraction of DNA and RNA from the PDOs

The PDOs were disrupted with 250 µl per well Accumax (Innovative Cell Technologies) and collected in a microtube. DNA was extracted using a DNeasy Blood & Tissue Kit (Qiagen), and RNA was extracted using an RNeasy Mini Kit (Qiagen). The concentration of the extracted nucleic acids was measured using a Qubit Fluorometer (Qiagen).

# Panel sequencing

Using the extracted DNA, we performed mutation analysis using a next-generation sequencer on approximately 400 genes that could be evaluated using the Comprehensive Cancer Panel (CCP). First, a library was constructed using the Ion AmpliSeq Comprehensive Cancer Panel (4477685, Thermo Fisher Scientific) and the Ion AmpliSeq Library Kit Plus (4488990, Thermo Fisher Scientific), according to the manufacturer's protocols. Library quantification was performed on a 4150 TapeStation system (Agilent Technologies) using a D1000 ScreenTape (5067–5582, Agilent Technologies). Using the prepared library,

sequencing was performed on an Ion GeneStudio S5 (Thermo Fisher Scientific) using the Ion 540 Kit-OT2 and Ion 540 Chip (A27753, A27765, Thermo Fisher Scientific), according to the manufacturer's protocols. The obtained BAM files were analyzed using an *in-house* pipeline. Sequence reads were mapped to the human genome reference sequence (GRCh38/hg38) using BWA (http://bio-bwa.sourceforge.net/bwa.shtml,Ver.0.7.17) and Bowtie2 (http://bowtie-bio.sourceforge.net/bowtie2/index.shtml,Ver.2.4.5). Variant calling was performed using Freebayes (https://github.com/ekg/freebayes, Ver.1.3.6), and annotation was performed using ANNOVAR(http://annovar.openbioinformatics.org). Sequence data with coverage > 50 were used for the analysis.

# Transcriptome analysis

A library was constructed using the extracted RNA with an Ion AmpliSeq Transcriptome Human Gene Expression Kit (A26325; Thermo Fisher Scientific) according to the manufacturer's protocol. Library quantification was performed on a 4150 TapeStation system (Agilent Technologies) using a D1000 ScreenTape (5067–5582, Agilent Technologies). Using the prepared library, sequencing was performed on an Ion GeneStudio S5 (Thermo Fisher Scientific) using the Ion 540 Kit-OT2 and Ion 540 Chip (A27753, A27765, Thermo Fisher Scientific), according to the manufacturer's protocols. RNA sequencing (RNA-seq) was analyzed using an *in-house* pipeline. The obtained sequence reads were mapped against the human genome reference sequence (GRCh38/hg38) using STAR (https://github.com/alexdobin/STAR, Ver.1.6.0), and gene-level transcript quantification and transcripts per million (TPM) calculations were performed using RSEM (https://github.com/deweylab/RSEM, Ver.1.3.3).

# Statistical analysis

Using the obtained log10(TPM), Pearson correlation analysis was performed with the normalized AUC values of each drug sensitivity analysis result, and genes were identified under the condition of $P\ value < 0.001$. Non-negative Matrix Factorization (NMF) analysis, a nonhierarchical clustering method, was used to extract genes associated with normalized AUCs representing drug sensitivity. Using the R package NMF (http://renozao.github.io/NMF/, Ver.0.26), NMF analysis was performed on the log10(TPM) of the identified genes (rank = 2). Based on the results of the NMF analysis, GO enrichment analysis and pathway enrichment analysis were performed on gene groups that were found to be associated with the normalized AUC values (adjusted P value < 0.05) using ClusterProfiler version 4.8.3, and ReactomePA version 1.44.0. Finally, we performed a regression analysis of the genes obtained from the enrichment analysis and normalized the AUC values.

# Declarations


### *Acknowledgments*

This study was supported by JSPS KAKENHI (grant number: JP23K07369).


### *Specific author contribution:*

Oyama S and Matsuda A conceived and planned the experiments. Oyama S, Nawa Y and Matsuda A performed the experiments. Oyama S and Matsuda A planned and conducted the simulations. Kakizaki Y, Ishizawa T, Kobayashi T, Nakamura H, Nawa Y, Otaki Y, Nagata Y and Honma S contributed to sample preparation. Sato H, Murakami Y, Oyama S, and Matsuda A processed the experimental data and performed the analyses. Oyama S, Matsuda A, Makino N, and Ueno Y contributed to the interpretation of the results. Oyama S, Matsuda A and Murakami Y took the lead in writing the manuscript. All of the authors provided critical feedback and helped shape the research, analysis, and manuscript.

### *Data availability statement*

The authors confirm that the data supporting the findings of this study are available within the article and its supplementary materials.

### Competing Interests

All of the authors declare no competing interests.

### *Additional Information*

**Supplementary Information** The online version contains supplementary material available at

# References


1. Siegel RL, Miller KD, Wagle NS, Jemal A. Cancer statistics, CA Cancer J. Clin., 73:17–48 (2023).
2. Tempero MA. et al. Pancreatic adenocarcinoma, version 2.2021, NCCN Clinical practice guidelines in oncology. J. Natl Compr. Canc. Netw.,19:439–457 (2021).
3. Sugimoto M. et al. Survival benefit of neoadjuvant therapy in patients with non-metastatic pancreatic ductal adenocarcinoma: A propensity matching and intention-to-treat analysis. J. Surg. Oncol., 120:976–984 (2019).
4. Katz MHG. et al. Efficacy of preoperative mFOLFIRINOX vs mFOLFIRINOX Plus hypofractionated radiotherapy for borderline resectable adenocarcinoma of the pancreas: The A021501 Phase 2 Randomized Clinical Trial. JAMA Oncol., 8:1263–1270 (2022).
5. Takahashi S, et al. Neoadjuvant S-1 with concurrent radiotherapy followed by surgery for borderline resectable pancreatic cancer: a phase II open-label multicenter prospective trial (JASPAC05). Ann. Surg., 276:e510-e517 (2022).
6. Grasso C, Jansen G, Giovannetti E. Drug resistance in pancreatic cancer: impact of altered energy metabolism. Crit. Rev. Oncol. Hematol., 114:139–152 (2017).
7. Lancaster MA, Knoblich JA. Organogenesis in a dish: modeling development and disease using organoid technologies. Science, 345:1247125 (2014).
8. Marsee A. et al. Building consensus on definition and nomenclature of hepatic, pancreatic, and biliary organoids. Cell Stem Cell, 28:816–832 (2021).

9. Boj SF. et al. Organoid models of human and mouse ductal pancreatic cancer. Cell, 160:324–338 (2015).
10. Lee JH. et al. Establishment of patient-derived pancreatic cancer organoids from endoscopic ultrasound-guided fine-needle aspiration biopsies. Gut Liver, 16:625–636 (2022).
11. Grossman JE. et al. Organoid sensitivity correlates with therapeutic response in patients with pancreatic cancer. Clin. Cancer Res., 28:708–718 (2022).
12. Seino T. et al. Human pancreatic tumor organoids reveal loss of stem cell niche factor dependence during disease progression. Cell Stem Cell, 22:454–467.e456 (2018).
13. Vincent A, Herman J, Schulick R, Hruban RH, Goggins M. Pancreatic cancer. Lancet, 378:607–620 (2011).
14. Ryan DP, Hong TS, Bardeesy N. Pancreatic adenocarcinoma. N. Engl. J. Med., 371:1039–1049 (2014).
15. Korc M. Driver mutations: a roadmap for getting close and personal in pancreatic cancer. Cancer Biol. Ther., 10:588–591 (2010).
16. Honeywell RJ, Ruiz van Haperen VWT, Veerman G, Smid K, Peters GJ. Inhibition of thymidylate synthase by 2',2'-difluoro-2'-deoxycytidine (gemcitabine) and its metabolite 2',2'-difluoro-2'-deoxyuridine. Int. J. Biochem. Cell Biol., 60:73–81 (2015).
17. Heinemann V, Hertel LW, Grindey GB, Plunkett W. Comparison of the cellular pharmacokinetics and toxicity of 2',2'-difluorodeoxycytidine and 1-beta-D-arabinofuranosylcytosine. Cancer Res., 48:4024–4031 (1988).
18. Huang P, Chubb S, Hertel LW, Grindey GB, Plunkett W. Action of 2' ,2' -difluorodeoxycytidine on DNA synthesis. Cancer Res., 51:6110–6117 (1991).
19. Huang P, Plunkett W. Induction of apoptosis by gemcitabine. Semin. Oncol., 22:19–25 (1995).
20. Brzovic PS, Rajagopal P, Hoyt DW, King MC, Klevit RE. Structure of a BRCA1-BARD1 heterodimeric RING-RING complex. Nat. Struct. Biol., 8:833–837 (2001).
21. Paull TT, Cortez D, Bowers B, Elledge SJ, Gellert M. Direct DNA binding by BRCA1. *Proc. Natl. Acad. Sci. U. S. A.*, 98:6086–6091 (2001).
22. Zhao W. et al. BRCA1-BARD1 promotes RAD51-mediated homologous DNA pairing. Nature, 550:360–365 (2017).
23. Zhu Y. et al. Tamoxifen-resistant breast cancer cells are resistant to DNA-damaging chemotherapy because of upregulated BARD1 and BRCA1. Nat. Commun., 9:1595 (2018).
24. Bian L, Meng Y, Zhang M, Li D. MRE11-RAD50-NBS1 complex alterations and DNA damage response: implications for cancer treatment. Mol. Cancer, 18:169 (2019).
25. Ewald B, Sampath D, Plunkett W. ATM and the Mre11-Rad50-Nbs1 complex respond to nucleoside analogue-induced stalled replication forks and contribute to drug resistance. Cancer Res., 68:7947–7955 (2008).

26. Kim YM. et al. PNUTS, a protein phosphatase 1 (PP1) nuclear targeting subunit. Characterization of its PP1- and RNA-binding domains and regulation by phosphorylation. J. Biol. Chem., 278:13819–13828 (2003).
27. Landsverk HB. et al. The protein phosphatase 1 regulator PNUTS is a new component of the DNA damage response. EMBO Rep., 11:868–875 (2010).
28. Yang X. et al. SRSF6 regulates alternative splicing of genes involved in DNA damage response and DNA repair in HeLa cells. Oncol. Rep., 44:1851–1862 (2020).
29. Palmieri F. The mitochondrial transporter family SLC25: identification, properties and physiopathology. Mol. Aspects Med., 34:465–484 (2013).
30. Palmieri F. Mitochondrial carrier proteins. FEBS Lett., 346:48–54 (1994).
31. Palmieri L, Palmieri F, Runswick MJ, Walker JE. Identification by bacterial expression and functional reconstitution of the yeast genomic sequence encoding the mitochondrial dicarboxylate carrier protein. FEBS Lett., 399:299–302 (1996).
32. Hlouschek J, Ritter V, Wirsdörfer F, Klein D, Jendrossek V, Matschke J. Targeting SLC25A10 alleviates improved antioxidant capacity and associated radioresistance of cancer cells induced by chronic-cycling hypoxia. Cancer Lett., 439:24–38 (2018).
33. Zhou X, Paredes JA, Krishnan S, Curbo S, Karlsson A. The mitochondrial carrier SLC25A10 regulates cancer cell growth. Oncotarget, 6:9271–9283 (2015).
34. Gallo KA, Johnson GL. Mixed-lineage kinase control of JNK and p38 MAPK pathways. Nat. Rev. Mol. Cell Biol., 3:663–672 (2002).
35. Marusiak AA. et al. Mixed lineage kinases activate MEK independently of RAF to mediate resistance to RAF inhibitors. Nat. Commun., 5:3901 (2014).
36. Xia J. et al. miR-7 suppresses tumor progression by directly targeting MAP3K9 in pancreatic cancer. Mol. Ther. Nucleic Acids., 13:121–132 (2018).
37. Fan YC, Hsu KC, Lin TE, Zechner D, Hsu SP, Tsai YC. Investigation of anti-tumor effects of an MLK1 inhibitor in prostate and pancreatic cancers. Biology (Basel), 10 (2021).
38. Tsai S. et al. Development of primary human pancreatic cancer organoids, matched stromal and immune cells and 3D tumor microenvironment models. BMC Cancer, 18:335 (2018).
39. Schuth S. et al. Patient-specific modeling of stroma-mediated chemoresistance of pancreatic cancer using a three-dimensional organoid-fibroblast co-culture system. J. Exp. Clin. Cancer Res.,41:312 (2022).

# Figures

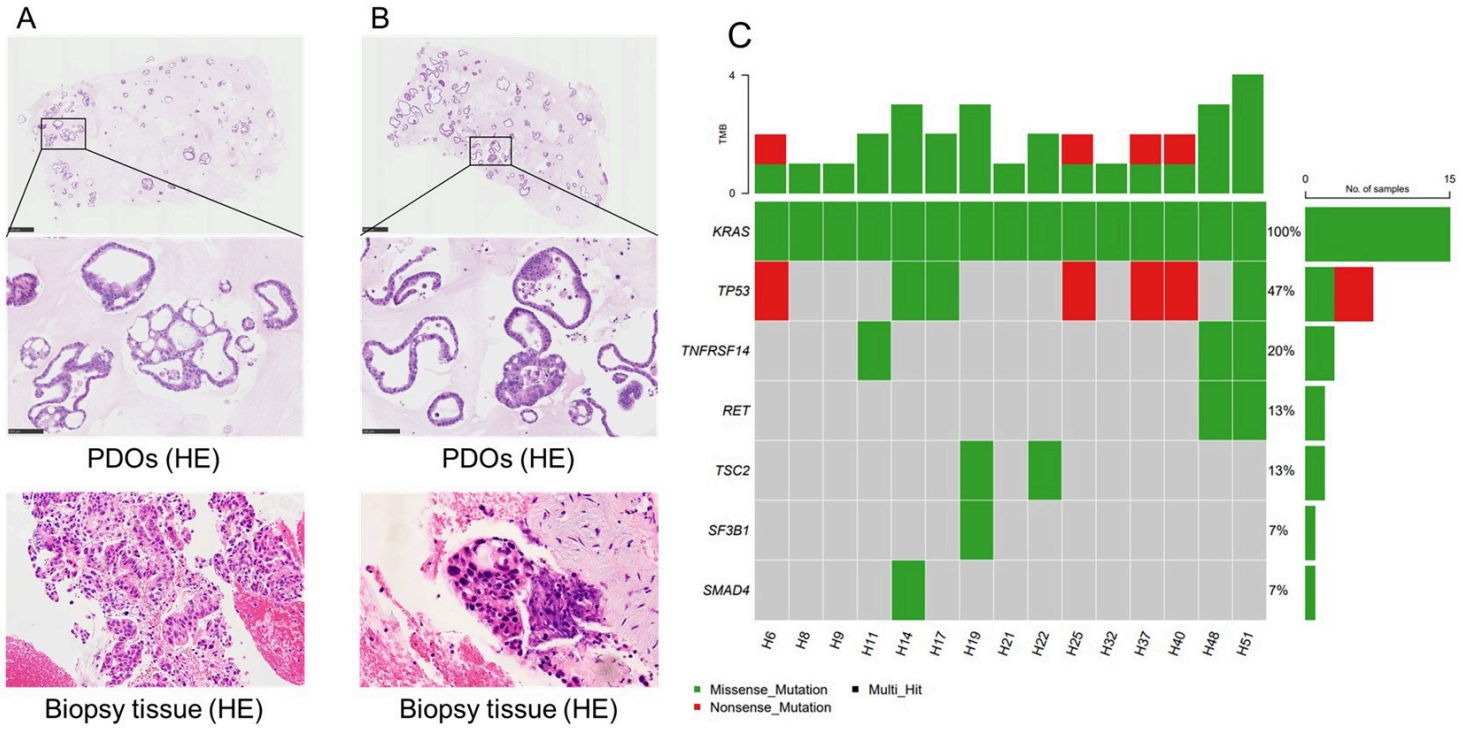


## Figure 1

### PDOs show pathological and genetic homology with donor tumor

A. HE stains image of the H8 case. Tumor cells with large nuclei and irregular ductal structures were observed, the findings were consistent with the HE staining image of the EUS-FNA specimen.

B. HE staining image of the H9 case. Similar to the H8 case, tumor cells with large nuclei and irregular ductal structures were observed, and the findings were consistent with the HE staining image of the EUS-FNA specimen.

Scale bars are 500 μm for weakly magnified A (top) and B (top), and 100 μm for strongly magnified images A (middle) and B (middle).

C. Mutation analysis was performed using next-generation sequencing of approximately 400 genes that were evaluated using the Comprehensive Cancer Panel (CCP) of 15 PDOs. All 15 PDOs harbored *KRAS* mutations. Other mutations were observed in *TP53* (47%), *TNFRSF14* (20%), *RET* (13%), *TSC2* (13%), *SF3B1* (7%), and *SMAD4* (7%). The vertical axis represents the mutated gene name, the horizontal axis represents the number of organoid samples; missense mutations are shown in green, and nonsense mutations are shown in red. Tumor mutation burden (TMB) is shown in the upper part of the graph.

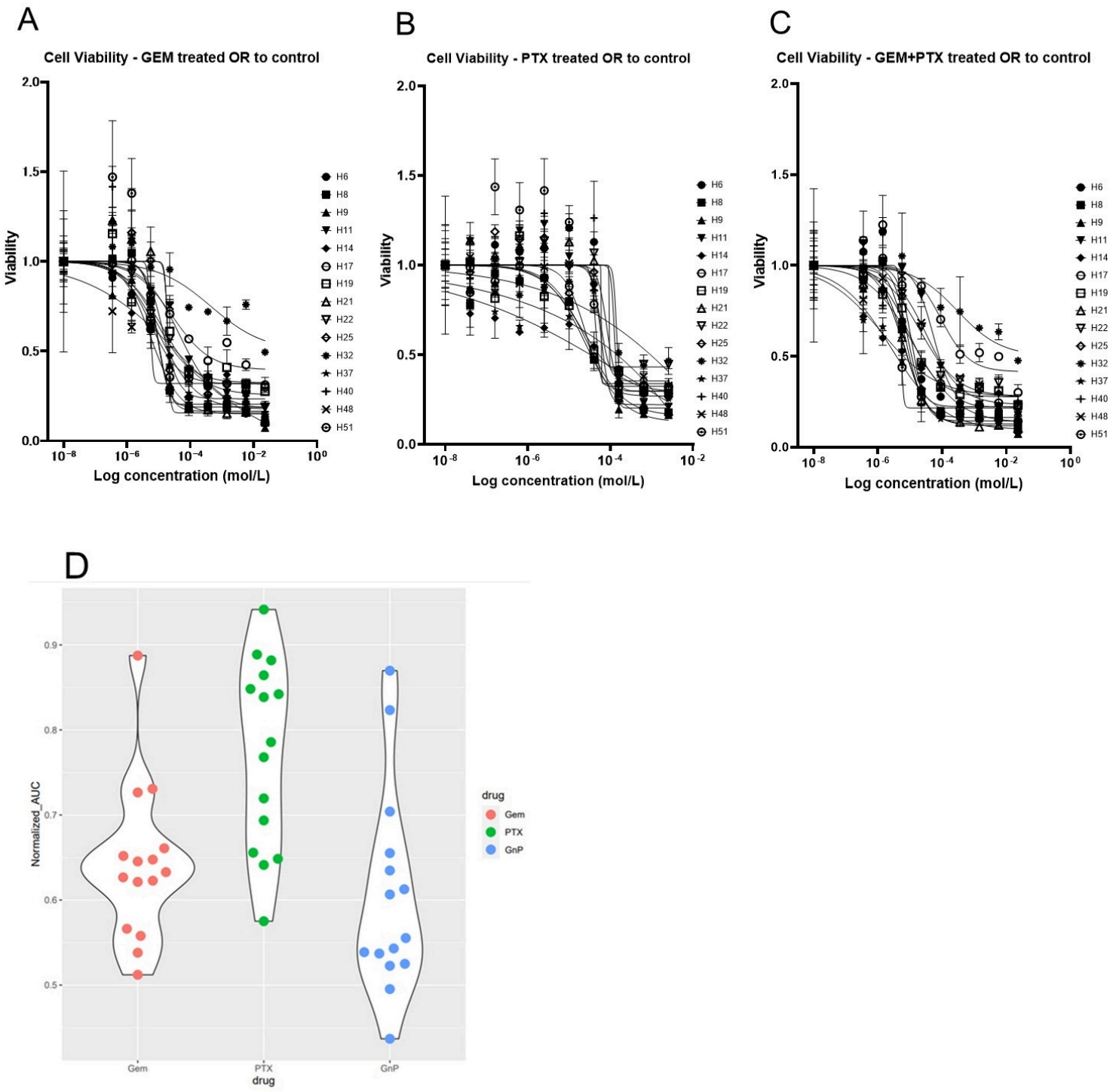


## Figure 2

### Drug sensitivity test results for PDOs

Drug sensitivity tests were performed on 15 PDOs derived from EUS-FNA specimens to evaluate their response to three chemotherapeutic drugs: GEM, PTX, and GEM + PTX.

A-C. Dose-response curves derived from cell viability. The vertical axis represents cell viability, the horizontal axis represents the logarithmically transformed drug concentration, and the dose-response

curves for GEM (A), PTX (B), and GEM + PTX (C) are shown. The dose-response curve of the PDOs differed among the organoid strains, indicating individual differences in drug sensitivity.

D. Violin plot obtained from Normalized AUC values for each drug. The vertical axis represents the normalized AUC value, and the horizontal axis represents the drug.

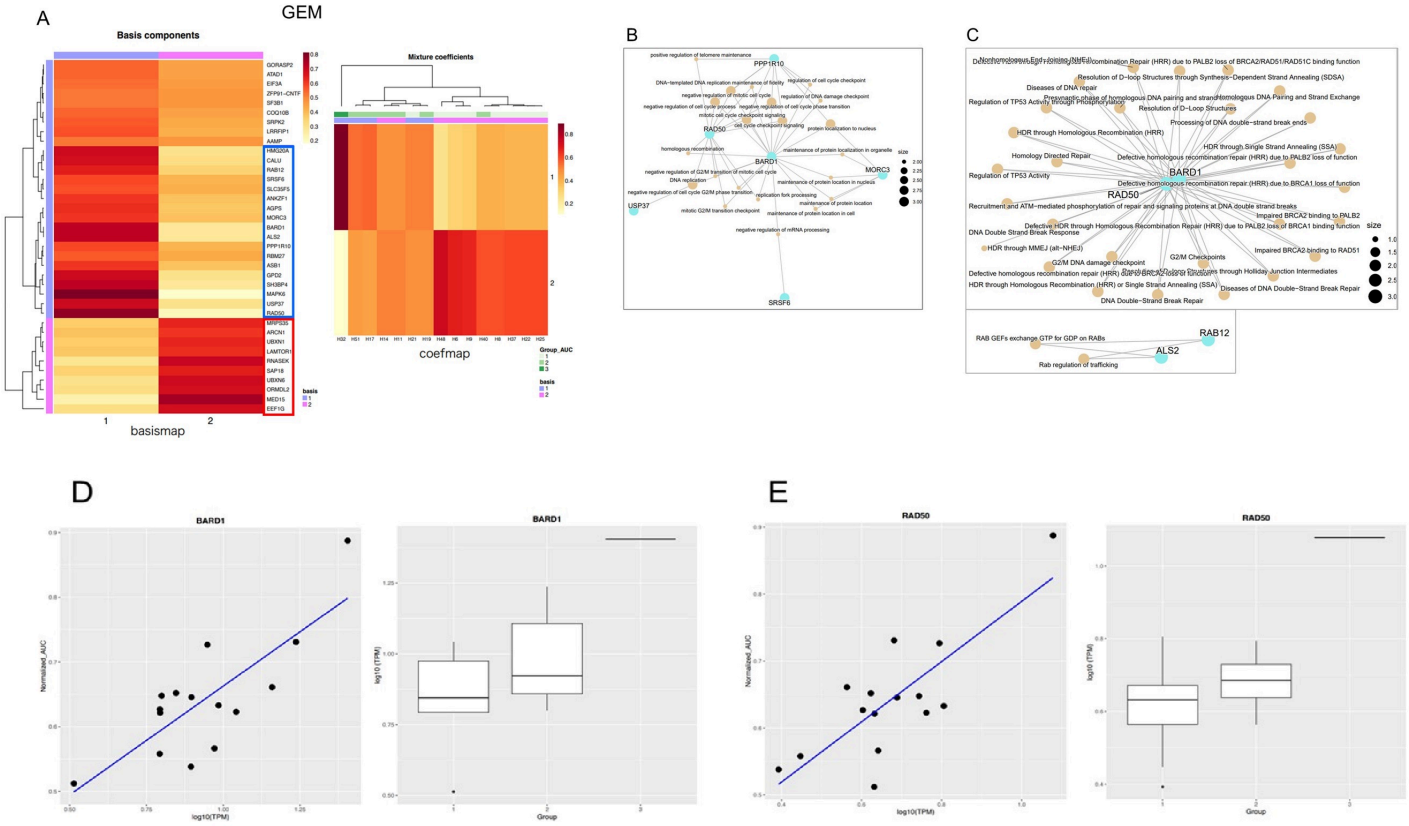


## Figure 3

### Drug sensitivity test and transcriptome analysis revealed the genes correlated to GEM resistance

Based on the gene expression profiles of the 15 PDOs by transcriptome analysis and the normalized AUC values in the drug sensitivity test, genes correlated with drug sensitivity were identified.

A. NMF analysis of 37 genes identified in the GEM group. The basis components were 37 genes on the vertical axis and two on the horizontal axis. The gene group framed blue is related to basis1, and the gene group framed red is related to basis2. For the mixture coefficients, the vertical axis represents the rank of 2, and the horizontal axis represents the PDOs sample. The relationships between each basis and normalized AUC values divided into three groups are shown, with basis 1 being associated with high normalized AUC values and basis 2 being associated with low normalized AUC values.

B, C. Gene concept network of GO enrichment analysis (B) and pathway enrichment analysis (C) of the basis1 gene group. GO enrichment analysis identified *BARD1, RAD50, PPP1R10, SRSF6, MORC3, and USP37.* Pathway enrichment analysis identified *BARD1, RAD50, RAB12, and ALS2.*

D, E. Regression analysis targeting *BARD1* (D) and *RAD50* (E) identified in enrichment analysis. The normalized AUC of each gene, *BARD1* or *RAD50*, is shown on the vertical axis, and log10 (TPM) on the horizontal axis. The regression line showed a positive slope, indicating that a high expression level was correlated with a high normalized AUC value. In the box-and-hide diagram, the vertical axis shows the log10(TPM) in each gene, and the horizontal axis shows the PDO groups divided into three groups according to the normalized AUC values, group1 had low AUC values, group2 had middle AUC values and group3 had high AUC values. It is shown that the group with a high normalized AUC value also has a high log10(TPM) value. For both *BARD1* and *RAD50*, the normalized AUC values correlated with gene expression levels, indicating that high expression levels of these genes correlate with GEM resistance.

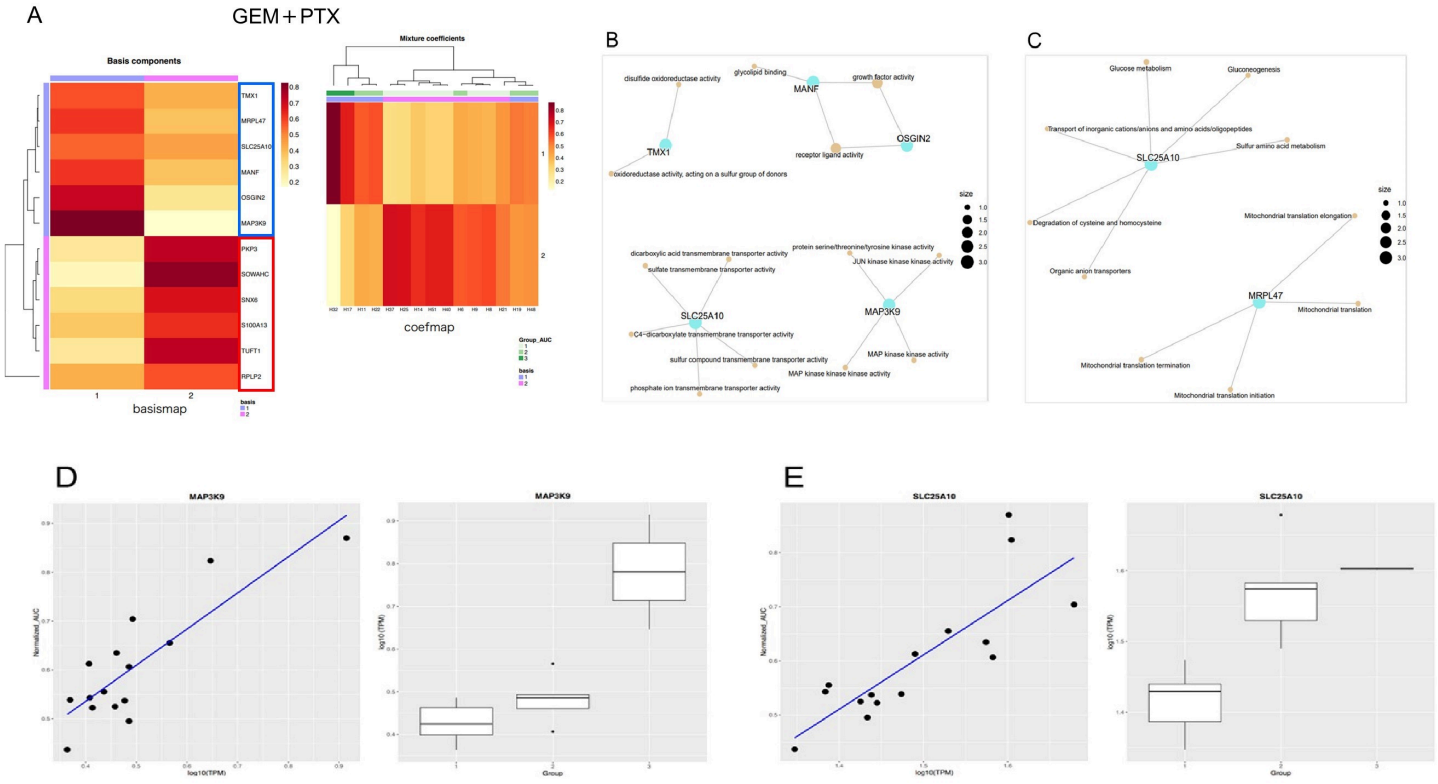


## Figure 4

### Drug sensitivity test and transcriptome analysis revealed the genes correlated to GEM + PTX resistance

A. NMF analysis results for 12 genes identified in the GEM+PTX group. Basis components are 12 genes on the vertical axis and rank of 2 on the horizontal axis. The gene group framed blue is related to basis1, and the gene group framed red is related to basis2. For the mixture coefficients, the vertical axis is rank of 2, and the horizontal axis is PDOs sample. The relationships between each basis and normalized AUC values divided into three groups are shown, with basis 1 being associated with high normalized AUC values, and basis 2 being associated with low normalized AUC values.

B, C. Gene concept network of GO enrichment analysis (B) and pathway enrichment analysis (C) performed on the basis1 gene group, which corresponded to a high normalized AUC value in the NMF

analysis (adjusted P-value < 0.05). GO enrichment analysis identified *SLC25A10, MAP3K9, TMX1, MANF,* and *OSGIN2.* The pathway enrichment analysis revealed that *SLC25A10* and *MRPL47.*

D, E. Regression analysis targeting *SLC25A10* (D) and *MAP3K9* (E) as identified by enrichment analysis. The normalized AUC of each gene, *SLC25A10* or *MAP3K9*, is shown on the vertical axis, and log10 (TPM) on the horizontal axis. The regression line showed a positive slope, indicating that a high expression level correlated with a high normalized AUC value. In the box-and-hide diagram, the vertical axis shows the log10(TPM) in each gene, and the horizontal axis shows the PDO groups divided into three groups according to the normalized AUC values, group1 had low AUC values, group2 had middle and group3 had high AUC values. It has been shown that the group with a high normalized AUC value also has a high log10(TPM) value. In both gene, *SLC25A10* or *MAP3K9*, normalized AUC values correlated with gene expression levels, indicating that high expression levels of these genes correlated with GEM + PTX resistance.

## Supplementary Files

This is a list of supplementary files associated with this preprint. Click to download.

- supplementaryTabless1s4.docx